Developments in the Built Environment 14 (2023) 100142

Contents lists available at ScienceDirect

Developments in the Built Environment

journal homepage: www.sciencedirect.com/journal/developments-in-the-built-environment

Non-destructive evaluation of the effects of exposure environment in mortars using non-linear ultrasonic measurements

José Marcos Ortega *, Marina Miró, Javier Ibáñez-Gosálvez, Antonio José Tenza-Abril

Departamento de Ingeniería Civil, Universidad de Alicante, Ap. Correos 99, Alacant/Alicante, 03080, Spain

ARTICLE INFO

Keywords:
Non-linear ultrasonic test
Non-destructive characterization
Real environment
Non-optimum condition
Microstructure

ABSTRACT

The development of non-destructive techniques has currently a high interest, such as those based on non-linear ultrasonic measurements. In this work it has been assessed the possible application of non-linear ultrasonic measurements for getting information related to the microstructure and properties of Portland cement mortars exposed to real and non-optimum environments. The pore structure was studied using mercury intrusion porosimetry and differential thermal analyses. Mechanical strengths and linear ultrasonic pulse velocity were determined. Regarding non-linear ultrasonic measurements, the results of parameters R and DIFA were analyzed. The tests were performed at 28 and 250 days. At later ages, a loss of microstructure refinement and a worsening of mechanical performance of the mortars were observed. The results of non-linear ultrasonic parameters R and DIFA overall agreed with those obtained for the microstructural and mechanical characterization performed. In particular, an adequate correlation between parameter DIFA and the pore size distributions was observed.

1. Introduction

The real construction elements are in contact with different environments. Therefore, the geographical location of buildings and other civil engineering works may influence the properties development of their constituent materials, in particular when cementitious materials are used (Ortega et al., 2017; Xue et al., 2021). These environmental conditions (Shattaf et al., 2001; V Venkata and Mahindrakar, 2017), such as temperature, relative humidity, rainfall and presence of aggressive substances, among others, could play a major role in the evolution of pore structure, durability and mechanical performance of these materials, thus having a direct influence in their service life (European Committee for Standardization, 2004). As a consequence, the evaluation of the behavior of these materials kept in real climate conditions (Thomas and Matthews, 2004; Thomas et al., 2008; Chalee et al., 2009) and non-optimum laboratory environments (Çakır and Aköz, 2008; Detwiler et al., 1991; Ramezanianpour and Malhotra, 1995) would be interesting, as well as the use of non-destructive techniques (Kogbara et al., 2015; Williams et al., 2017; Ghosh and Tran, 2015, 2015de Grazia et al., 2021) for studying their properties when they are subject to these harmful conditions. Nowadays, the development of techniques for non-destructive testing (NDT) has a high interest, in particular those that could be used for the inspection of structures.

Elastic wave methods have been frequently applied in the field of NDT for evaluating the mechanical performance and for the detection of pathologies in structures and materials. The propagation of waves along a material (i.e. concrete), is reactive to the presence of discontinuities or other defects (voids, cracks, etc.), or material development properties. The most important wave-based methods for evaluating damages in structures made with concrete are: acoustic emission (AE) (Ospitia et al., 2023), impact echo (IE) (Fülöp et al., 2022), ultrasonic pulse velocity (UPV) (Revilla-Cuesta et al., 2022), surface-wave techniques (Lefever et al., 2022, 2023; Ahn et al., 2018, 2022a; In et al., 2015) and diffuse-wave techniques (Quiviger et al., 2012; Payan et al., 2013; In et al., 2017; Zhang et al., 2018; Ahn et al., 2022b) for monitoring and evaluation of healing, cracks or discontinuities in concrete.

Measurements obtained by ultrasonic waves allow the evaluation of some durability indicators. Ultrasonic pulse velocity measurement is one of the simplest non-destructive testing methods and it is extensively applied in construction industry (Del Río et al., 2004; Ohdaira and Masuzawa, 2000). The UPV is used to estimate the mechanical strength and for the characterization and classification of concrete, as well as for assessing internal defects and concrete thickness (Ohdaira and Masuzawa, 2000). In addition, there are several theoretical models which allow predicting the relationships between UPV and other physico-mechanical parameters. Several examples of these parameters

* Corresponding author.
E-mail address: jm.ortega@ua.es (J.M. Ortega).

https://doi.org/10.1016/j.dibe.2023.100142
Received 22 November 2022; Received in revised form 1 March 2023; Accepted 4 March 2023
Available online 6 March 2023

are permeability (Panzera et al., 2008; Lafhaj et al., 2006), density (Panzera et al., 2008), modulus of elasticity (Trtnik et al., 2008; Yildirim and Sengul, 2011), and porosity (Lafhaj et al., 2006). Additionally, the effects of the water/cement ratio (Lafhaj et al., 2006), the particle size of the aggregates (Berriman et al., 2005; Tanyidizi and Coskun, 2008), the hydration process (Trtnik et al., 2008; Zhang et al., 2009) and the curing conditions (Zhang et al., 2009) have been investigated and modeled by numerous researchers as a function of the UPV.

Non-linear ultrasonic techniques (NLU) show promise for the research of non-linear dynamic properties of structures and materials because of their enhanced detection of features related to pore structure within materials. The existence of defects on a wide scale range (from nanoscale to macroscale) enhances non-linear acoustic phenomena (Eiras, 2016; Climent et al., 2022). Overall, materials whose mechanical behavior has a high dependence on the quality of the bond between their constituents fall into the non-linear mesoscopic elasticity (NMEM) class (Guyer and Johnson, 2009). Common examples of these materials are rocks, soil, concrete, damaged materials and granular media. In these materials, the elastic waves interact with heterogeneities and defects, producing non-linear acoustic phenomena, that may be used for non-destructive evaluation (Kundu et al., 2019) or for establishing damage thresholds (Miró et al., 2021). Between those phenomena, it is noteworthy to highlight the amplitude and frequency wave modulations (Warnemuende and Wu, 2004; Chen et al., 2019; Den Abeele et al., 2000a; Climent-Llorca et al., 2020), higher harmonic generation (Shah and Ribakov, 2009; Kim et al., 2014; Stauffer et al., 2005; Scalerandi et al., 2013; Climent et al., 2019) and amplitude-dependent resonant frequency and attenuation shifts (Van Den Abeele and De Visscher, 2000; Payan et al., 2007; Eiras et al., 2018).

Then, the purpose of this research is to evaluate the possible application of non-linear ultrasonic measurements (Miró et al., 2021; Climent-Llorca et al., 2020; Climent et al., 2019) for obtaining information about properties and microstructure of mortars exposed to different environmental conditions. These conditions were a real outdoor Mediterranean climate environment and a non-optimum laboratory environment with low relative humidity. In addition, a group of specimens were stored in an optimum laboratory condition. The results of the parameters obtained from non-linear ultrasonic measurements were compared to pore structure characterization of the mortars, performed with mercury intrusion porosimetry and differential thermal analysis, and with their mechanical strengths and classical linear UPV results.

2. Experimental setup

2.1. Materials and preparation of samples

Mortars have been tested. They were made with an ordinary Portland cement CEM I 42.5 R (AENOR and UN E-EN 197–1:2011, 2000). The aggregate/cement ratio was 3 and the water/cement ratio used was 0.5. The fine aggregate accomplished the prescriptions of UNE-EN 196-1 standard (AENOR and UNE-EN 196–1:2005, 2005).

Prisms with dimensions 4 cm × 4 cm x 16 cm were made, being kept at 20 °C temperature and 95% relative humidity in a chamber along their initial 24 h since setting. The specimens were de-moulded after that time. Lastly, the testing ages were 28 and 250 days.

2.2. Environmental conditions

Three environments were studied. The first one was an optimum laboratory environment, in which the mortar specimens have been placed in a chamber with 100% relative humidity and 20 °C temperature. It was named as environment A.

The second environment consisted of placing the mortar specimens in a real outdoor exposure station. This condition was called environment B. The exposure station was in the town of Orxeta (38° 33′ 47″ N, 0° 15′ 43″ W, 177 m.a.s.l.), being placed at 10 km from the coast. This town belongs to the province of Alicante, in the southeast of Spain. Therefore, the mortar samples were matured under a real Mediterranean climate condition without weather conditions protection. This environment would be compatible with the prescriptions of exposure class XC4 (corrosion induced by carbonation, cyclic wet and dry) according to the Eurocode 2 (European Committee for Standardization, 2004). Testing period covered from February to October. Along this time, the temperatures were mild. The relative humidity presented noticeable variability. Total rainfall registered during the exposure period was 212.5 mm, of which 86 mm were registered in the first 30 days and 176 mm in the first 90 exposure days. The daily average humidity and temperature in the site are represented in Figs. 1 and 2, respectively. Mortar samples of this condition B were cured during 7 days before being moved to the exposure station (Thomas et al., 2008; Ramezanianpour and Malhotra, 1995).

The third environment consisted of a non-optimum laboratory condition, which was designated as environment C. In this condition, the mortars have been exposed to a constant 65% relative humidity and 20 °C temperature. The values of these parameters were chosen because they are the annual average values of relative humidity and temperature registered for the eastern coast of Spain, with Mediterranean climate. For reaching these values, the mortar samples matured in contact with this environment C, were introduced in hermetically sealed boxes with glycerol solutions, prepared following the prescriptions of the DIN 50 008 part 1 standard (für N. E.V, 1981) for achieving the adequate 65% value of relative humidity. Finally, these boxes were stored into a chamber with controlled 20 °C temperature.

2.3. Mercury intrusion porosimetry

Mercury porosimetry is a popular technique for characterizing the pore network of different types of materials (Diamond, 2000; Ouellet et al., 2007; Horpibulsuk et al., 2010). This test was performed using a Poremaster-60 GT porosimeter (Quantachrome Instruments). Specimens were dried at 50 °C over a 48-h period of time before the beginning of the test. In this work, pore size distributions and total porosity were analyzed. The distribution of pores by sizes was established considering this intervals: <10 nm, 10–100 nm, 100 nm to 1 μm, 1–10 μm, 10 μm to 0.1 mm, and >0.1 mm (Pedeferri and Bertolini, 2000; Ho et al., 2018). Two tests were made on the mortars for each environment at both maturing ages. The specimens tested were pieces obtained from prisms with dimensions 4 cm × 4 cm x 16 cm.

2.4. Differential thermal analysis

The differential thermal analyses were performed with a simultaneous TG-DTA model TGA/SDTA851e/SF/1100 manufactured by Mettler Toledo, which allows working from room temperature to 1100 °C. The heating ramp chosen consisted of 20 °C/min until 1000 °C in atmosphere of N2. The curve weight derivate versus temperature has been obtained. Three measurements were made on the mortars exposed to each environment studied at both testing ages. The powder samples used for this experimental technique have been obtained from milling pieces taken from prisms with dimensions 4 cm × 4 cm x 16 cm.

2.5. Mechanical strengths

The flexural and compressive strengths were determined following the standard UNE-EN 1015–11 (AENOR and UNE-EN 1015-1 1:1999, 1999). For each environment, three prismatic specimens have been tested at 28 and 250 days.

2.6. Ultrasonic pulse velocity

The ultrasonic pulse velocity was obtained following the standard UNE-EN 12504–4 (AENOR and UNE-EN 12504-4, 2006). The time of

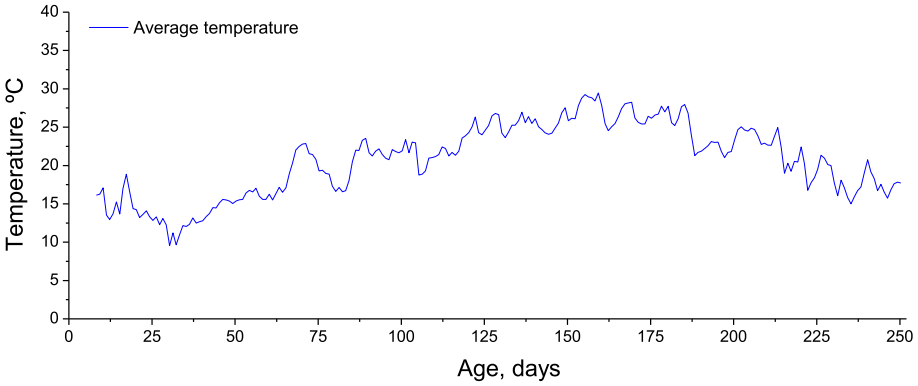

Fig. 1. Daily average temperature registered for environment B throughout the studied time period.

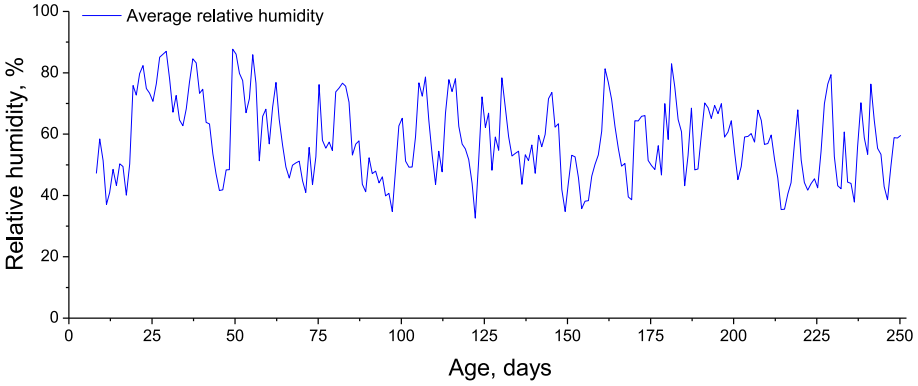

Fig. 2. Daily average relative humidity registered for environment B along the exposure time period.

propagation for ultrasonic waves along the highest size of the prism (16 cm) was determined using direct transmission. Test equipment Pundit Lab model (Proceq) with contact transducers, emitting ultrasonic pulses at 54 kHz, was used for performing the measurements. With the propagation time and the length of the prism, it has been calculated the ultrasonic pulse velocity. At 28 and 250 days, three prismatic specimens were tested for each environment and three determinations were performed on each specimen.

2.7. Non-linear ultrasonic measurements

With regard to the non-linear ultrasonic (NLU) technique, two pure tones ($f_0 = 20$ kHz and $f_1 = 200$ kHz) were simultaneously supply using two transducers. A signal generator (SONY AFG310) was used for the emission of the high-frequency probe signal at 5 V of amplitude. The low-frequency pump was generated with a 16-bit ADC resolution I/O device NI-USB 6361, which was also used for the acquisition of the frequency modulated signal (sampling frequency of 2 MHz). As microcracking detection depends significantly on the frequency and energy of the pump wave, an amplifier FS WMA-100 was used for feeding the pump wave signal, which was transmitted using a Langevin transducer working at his resonance frequency of 20 kHz. The input voltage (after amplification) was set to 140 V. The high-frequency signal was received and emitted with two broadband ultrasonic transducers IDK09 (Dakel, 2022), see Fig. 3. The coupling agent was white soft paraffin (Acofarma).

The Fast Fourier Transform algorithm was used for transforming the signal registered to the frequency domain. The mechanical non-linearity of a system gives rise to additional sidebands output frequency components. Otherwise, if the system behaves linearly, the sideband frequencies are not generated. The frequencies at which IMD occurs are the difference and/or the sum of integer multiples of the fundamental frequencies. The amplitude of the sidebands with regard to the amplitudes

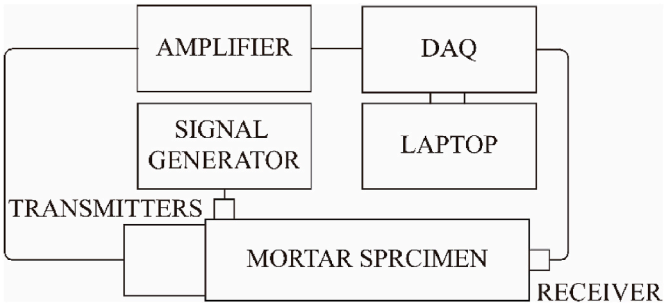

Fig. 3. Experimental setup used for the nonlinear ultrasonic measurements and relative positions of the transducers: Langevin emitter (f_0), IDK emitter (f_1), and IDK receiver.

of the pump and probe waves enable the quantification of the non-linear constitutive elastic properties (Den Abeele et al., 2000a) or the detection of localized defects (cracks) (Climent et al., 2022; Miró et al., 2021; Climent-Llorca et al., 2020; Wu and Warnemuende, 2005; Donskoy et al., 2001). Therefore, the probe amplitudes (f_1) and the frequencies of intermodulation first-order ($f_1 \pm f_0$) and second-order ($f_1 \pm 2f_0$) were used to assess the non-linear parameters R (intensity modulation ratio) and DIFA (difference of amplitudes), see Ec. (1) and (2). Fig. 4 shows a schematic representation of the non-linear wave modulation effect for a non-linear system.

The intensity modulation ratio, R, used in many studies as the damage index (Miró et al., 2021; Pieczonka et al., 2016; Den Abeele et al., 2000b; Muller et al., 2005; Aymerich and Staszewski, 2010), is defined as:

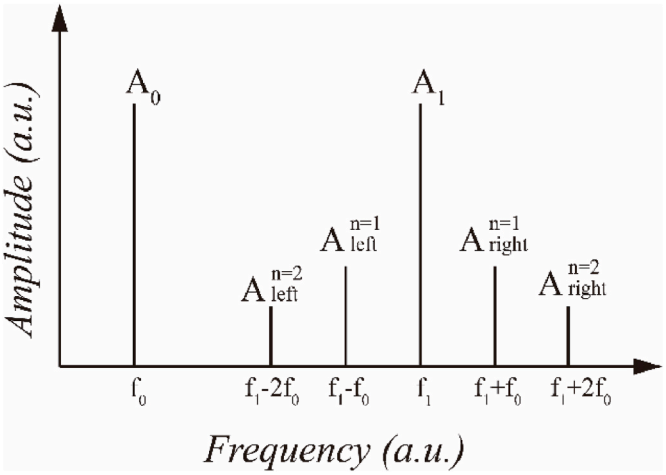

Fig. 4. Schematic representation of the spectrum resulting from a Nonlinear Wave Modulation Spectroscopy test (Miró et al., 2021).

$$R = \frac{\sum_{n=1}^{N}\left(A_{left}^{n} + A_{right}^{n}\right)}{A_1} \quad (1)$$

A short time ago, a new parameter has been proposed for getting information about the micro-damage through the intermodulation nonlinear features. This new parameter was named as DIFA (difference of amplitudes), being considered in order to represent the redistribution of elastic energy between the fundamental frequency component and the various intermodulation products, generated when the elastic wave travels through the medium in which there is presence of critical micro-defects (Climent et al., 2022; Climent-Llorca et al., 2020). This parameter is defined as:

$$DIFA = A_1 - \sum_{n=1}^{N}\left(A_{left}^{n} + A_{right}^{n}\right) \quad (2)$$

where A_{left}^{n} and A_{right}^{n} consisted of the amplitudes of the N sideband intermodulation products, and A_1 is the amplitude of the fundamental high-frequency probe. In this research, the first-order ($A_{f1\pm f0}$) and second-order ($A_{f1\pm 2f0}$) intermodulation products were only taken into consideration for determining the values of both R and DIFA parameters (N was set to 2). When there is a boost in the non-linear characteristics, for example crack development, it is produced the increase of parameter R and decrease of DIFA.

Finally, at both testing ages, three samples were tested for each environment and three measurements were performed on each sample.

3. Results

3.1. Mercury intrusion porosimetry

The results of total porosity are depicted in Fig. 5. The lowest porosities were overall noted for environment A along the time period studied. At 28 days, it was similar for specimens exposed to environment A and B, whereas it was higher for those stored in environment C. From 28 to 250 days, this porosity scarcely modified for environments A and C, whereas it notably rose for condition B. At 250 days, the greatest porosity was obtained under non-optimum conditions, with scarce differences between both.

The distributions of pores by size obtained for the tested mortars have been represented in Fig. 6. A similar volume of pores <100 nm were noted at 28 days for those exposed to conditions A and B, though the volume of pores with sizes in the interval <10 nm was more noticeable for environment B. At early ages, samples matured in condition C also showed similar volume of finer pores (intervals <10 nm and 10–100 nm), although it presented higher volume of pores with diameters >100 nm, in comparison to the other conditions. From 28 to 250 days, it has been noted a rise of volume of pores <10 nm for specimens matured under condition A. On the contrary, samples kept in conditions B and C presented a drop of the volume of voids with diameters <100 nm, although greater volume of finer pores (interval <10 nm) was noted for condition B. In addition, an increase of the volume of pores with sizes >100 nm has been noted for conditions B between 28 and 250 days.

3.2. Differential thermal analysis

The curves derivate of weight versus temperature curves noted for the different conditions at 28 and 250 exposure days can be observed in Figs. 7 and 8, respectively. The peak due to decomposition of portlandite ($Ca(OH)_2$) can be observed in the range 450°C-550 °C (Taylor, 1997; Escalante-Garcia, 2003; Kjellsen et al., 1991), whereas the peak of carbonates ($CaCO_3$) decomposition is in the interval 700°C-750 °C (Taylor, 1997; Shui et al., 2008). At both ages, the highest area of portlandite peak was observed for environment A, and it increased with hardening age. For non-optimum environments, this area reduced with age, being this drop more appreciable for environment B than C. With regard the carbonates ($CaCO_3$) peak, its area rose with time for non-optimum environments, especially for environment B.

3.3. Mechanical strengths

The compressive and flexural strength results are respectively represented in Figs. 9 and 10. Both strengths hardly differed between environments A and B at 28 days, presenting smaller values for condition C. Between 28 and 250 days, these strengths increased for environment A, whereas it decreased for samples matured under environment B, keeping practically constant for condition C. At the last testing age, the

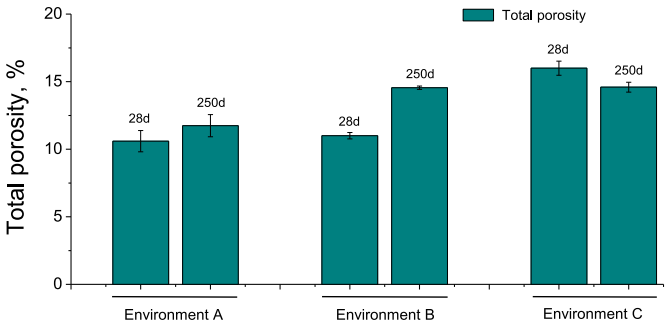

Fig. 5. Total porosity results noted for the exposure conditions studied.

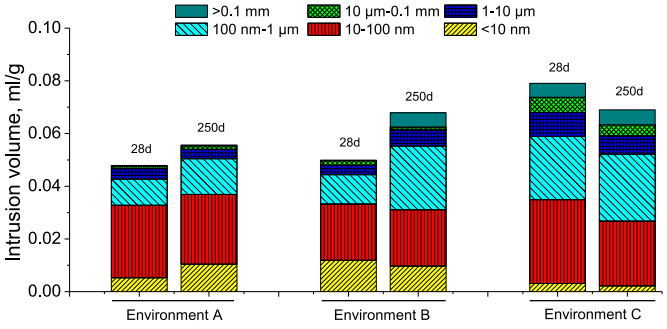

Fig. 6. Pore size distributions for the analyzed environments.

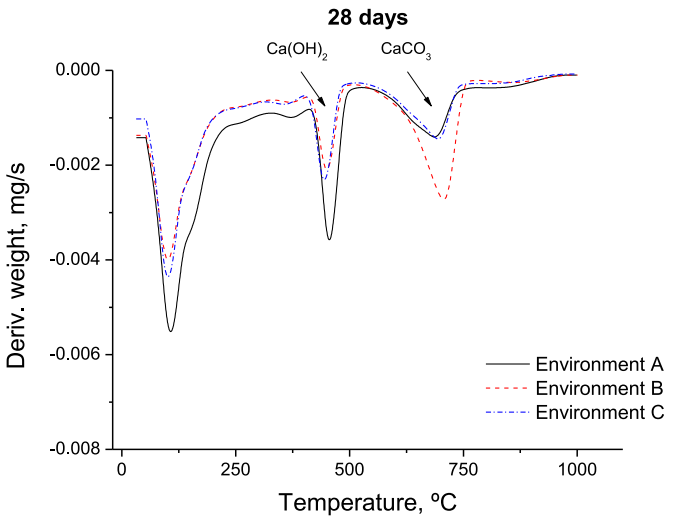

Fig. 7. Curves derivate of weight versus temperature for the different exposure environments at 28 days.

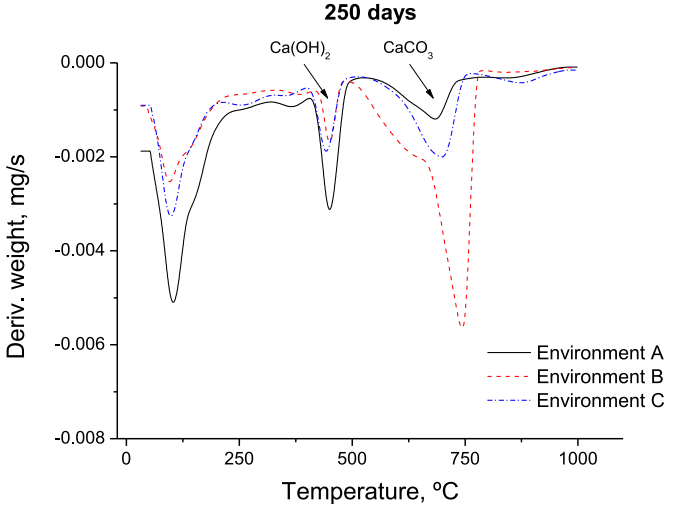

Fig. 8. Curves derivate of weight versus temperature for the mortars exposed to the environmental conditions studied at 250 days.

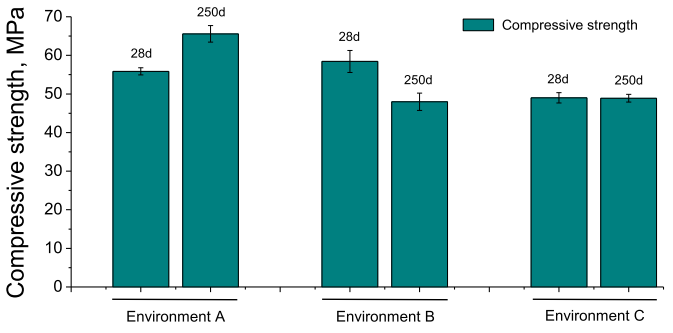

Fig. 9. Compressive strength results noted for the exposure environments.

highest compressive and flexural strengths corresponded to environment A. Comparing both non-optimum conditions, the long-term compressive strength showed similarities for environments B and C, while the flexural strength was lower for environment B in comparison with C.

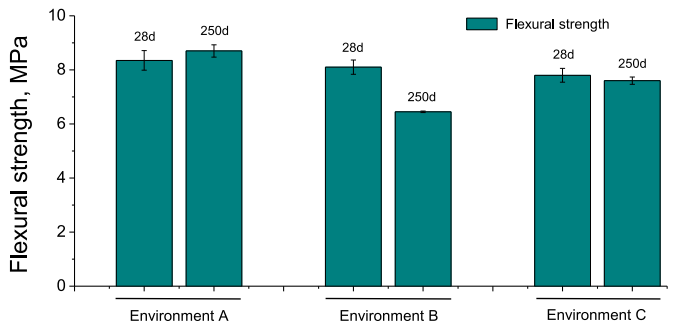

Fig. 10. Evolution of flexural strength obtained for the analyzed conditions.

3.4. Ultrasonic pulse velocity

The UPV results are depicted in Fig. 11. It showed scarce differences between the exposure environments at 28 days. The ultrasonic pulse velocity increased during the studied time period for mortars matured in environment A, whereas it kept practically constant for those exposed to non-optimum conditions.

3.5. Non-linear ultrasonic measurements

The results of parameter R are shown in Fig. 12. It hardly rose with age for samples matured under condition A. However, the growth of this parameter was more noteworthy for non-optimum conditions, showing higher values at 250 days for condition B compared to C.

The results of parameter DIFA have been depicted in Fig. 13. It was slightly higher at 28 days for mortars matured in environment B in comparison to A, whereas it was lower for condition C. From 28 to 250 days, it fell for non-optimum environments, and hardly changed for condition A, which showed the highest values of parameter DIFA at the last testing age.

4. Discussion

4.1. Mercury intrusion porosimetry and differential thermal analysis

Firstly, with regard to the mercury porosimetry (Figs. 5 and 6), the lower porosity values overall registered in environment A may be related to the high humidity of that optimum condition, which may allow a high progress of clinker hydration (Çakır and Aköz, 2008; Taylor, 1997), as indicated the increase of the portlandite peak area observed using differential thermal analyses (see Figs. 7 and 8). This also led to a higher microstructure refinement in the long term, which would be suggested by the greater proportion of pores of the smaller diameter interval at later ages in the case of this condition, compared to the other environments.

In environment B, where the materials were matured under a real outdoor condition, at early ages total porosity was relatively low and the

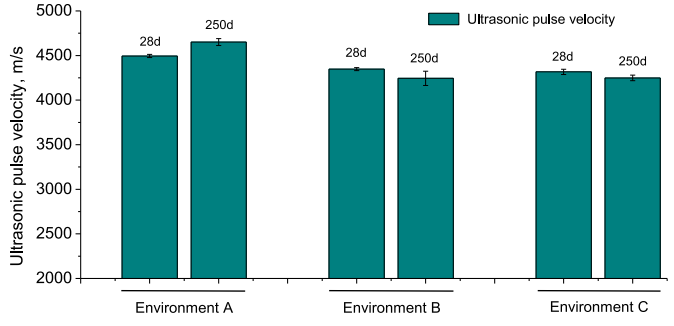

Fig. 11. Results of UPV noted for mortars exposed to the studied environments.

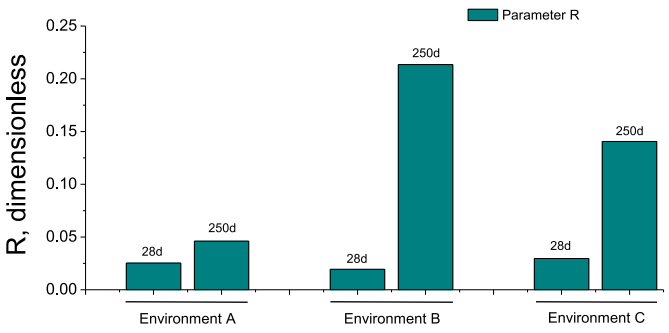

Fig. 12. Results of parameter R determined from non-linear ultrasonic measurements.

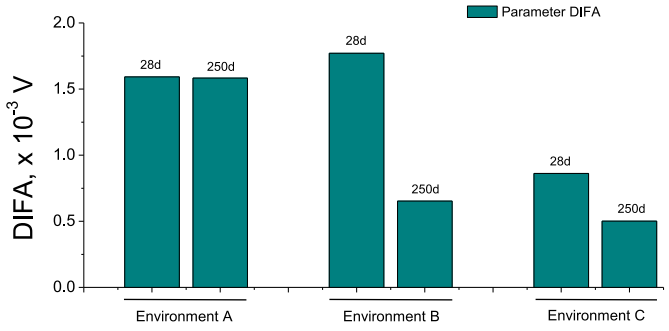

Fig. 13. Results of parameter DIFA based on non-linear ultrasonic measurements.

pore structure was more refined compared to environment A. It could be mainly due to the fact that during the first 28 days of exposure there was relatively abundant rainfall in the site, producing a relatively high humidity of the environment. This would have favoured the progress of hydration reactions of clinker (Çakır and Aköz, 2008), producing a noticeable formation of solid phases, giving as a result a considerable closing of microstructure, with high presence of finer pores. In this environment B, the total porosity experienced a notable increase at 250 days, which may be due to the effects of the higher temperatures and lower humidity to which the material was exposed in the long term. On one hand, this could cause the development of shrinkage (MA et al., 2007; Kanna et al., 1998), resulting in higher porosities and in a reduction of refinement of pore structure, revealed by the evolution of size distributions (see Fig. 6). Additionally, the possible development of carbonation at later ages could have also influenced these results, as would suggest the notable increase with time of area of carbonates peak in environment B, according to differential thermal analyses (see Figs. 7 and 8). Furthermore, the shortage of water in this real exposure condition could make difficult the long-term development of clinker hydration, avoiding the microstructure evolution towards a high proportion of finer pores.

In relation to the non-optimum laboratory environment C, the porosities were higher and the microstructure was less refined than in the other environments since early ages. This result may be caused by a slower development of clinker hydration (Çakır and Aköz, 2008; Taylor, 1997), in combination with the possible development of shrinkage at high maturing times (MA et al., 2007; Kanna et al., 1998), because of the low constant relative humidity of this environment mainly compared to the optimum condition.

4.2. Compressive and flexural strength

Regarding the mechanical properties (see Figs. 9 and 10), the higher values of compressive and flexural strengths, and their rise with time in general noted for environment A, especially in the long term, were compatible with microstructure characterization results previously discussed. In this optimum condition, the presence of a higher relative humidity favoured the development of the clinker hydration reactions (Çakır and Aköz, 2008; El-Dieb, 2007; Bingöl and Tohumcu, 2013), which leads to greater values of the mechanical parameters. On the contrary, in environments B and C, with a lower relative humidity, the development of these reactions at later ages would be slower (Çakır and Aköz, 2008; Taylor, 1997), as was already discussed for porosimetry results. Furthermore, this could also lead to the development of shrinkage cracking at later ages (MA et al., 2007; Kanna et al., 1998), resulting in lower flexural and compressive strengths, as was observed. The possible development of carbonation in environment B, suggested by the increase of carbonates peak, revealed by differential thermal analyses, could have also influenced in the reduction with time of mechanical strengths in this environment (Atiş, 2003; Khan and Lynsdale, 2002). The relative high strength values observed for condition B at 28 days, in comparison with environment A, would be a consequence of the high environmental humidity produced by the rainfall registered in the first exposure weeks in the station, agreeing with the discussed short-term microstructural results.

4.3. Ultrasonic pulse velocity

The lower differences between the analyzed environments observed with ultrasonic pulse velocity (see Fig. 11) would suggest that the presence of defects or damages in the mortars was not notable. Despite that, the increasing tendency with time of UPV reported for environment A would coincide with the growth of strengths and the progressive refinement of pores observed for mortars kept under this condition. In addition, the slight decreasing trend of ultrasonic pulse velocity for specimens matured in conditions B and C, as well as their lower long-term values in comparison with condition A, would overall agree with the reduction of pore refinement with age reported for these non-optimum environments, and their smaller flexural and compressive strengths at 250 days. Furthermore, the role played by the relative humidity of the samples throughout the studied time period is important when analysing these results, since while environment A increased the UPV over time, environments B and C decreased it, which would be in agreement with other authors (Biondi et al., 2017; Lencis and Korjakins, 2013).

4.4. Non-linear ultrasonic measurements

With regard to the NLU measurements, the lower values of parameter R (see Fig. 12) at 28 days noted for environment B would indicate a more linear system (Miró et al., 2021; Climent-Llorca et al., 2020), suggesting a more compact pore structure, which would be compatible with the higher percentage of finer pores and greater compressive strength observed for this environment in comparison with conditions A and C. The noticeable rise with time of parameter R noted for environment B, and to a lesser extent for environment C, and its higher values at 250 days compared to condition A, would indicate that the system became less linear (Miró et al., 2021; Climent-Llorca et al., 2020), revealing the possible development of long-term shrinkage cracking and a reduction of the refinement of pore network for the specimens kept in these non-optimum environments. This result would be also in keeping with porosimetry and mechanical strength results, which was explained in relation to the effects at later ages of lower environmental relative humidity present in environments B and C. Moreover, the effect of humidity on the non-linearity parameters is a highly influential factor (Payan et al., 2010). In particular, it has been reported that the non-linearity of the material is very high at very low humidity, so the higher long-term values of parameter R for environments B and C would be also consistent with the results reported by other authors (Payan et al., 2010).

In the case of parameter DIFA (see Fig. 13), also determined from non-linear ultrasonic measurements, its higher values for condition B at 28 days would show that the system was more linear (Climent-Llorca et al., 2020), entailing a closer microstructure. This would be in line with the higher refinement of pore network at 28 days observed for mortars stored in environment B. The parameter DIFA in the short term was greater in the case of environment A compared to condition C, indicating a less linear system in this last environment (Climent-Llorca et al., 2020), which would mean the presence of a coarser microstructure. This would coincide again with the distributions of pores by size at 28 days, in whose results mortars exposed to environment A showed higher proportion of voids with diameters belonging to the intervals <10 nm and 10–100 nm than those matured in condition C.

The decreasing tendency of parameter DIFA between 28 and 250 days for non-optimum environments would indicate that system evolved to less linear (Climent-Llorca et al., 2020), suggesting a loss of microstructure refinement, again agreeing with the changes of pore size distributions of the samples in conditions B and C. This reduction with time of proportion of finer pores of the abovementioned environments was justified in terms of the lower relative humidity at later ages, leading to the formation of shrinkage microcracks (MA et al., 2007; Kanna et al., 1998). Comparing the results of parameter DIFA at 250 days between environments B and C, it was higher for the first one. In view of this result, the system would be more linear (Climent-Llorca et al., 2020) for environment B, so it would be expected a finer microstructure in the mortars matured in this condition. This may be also compatible with the results of distributions of pores by size, because mortars kept in environment B presented a greater pore refinement at 250 days that those exposed to condition C. Therefore, it is noteworthy to highlight the noticeable correlation between the results of parameter DIFA and the pore size distributions determined with porosimetry, which would suggest that this parameter DIFA could be useful for getting reliable information about the microstructural evolution of cementitious materials, at least under the analyzed environmental conditions. With regard to the comparison between parameters R and DIFA, the differences between them come from their own definition. Indeed, there is a clear non-linear system at 28 days for environment C, which is very evident in the DIFA parameter, being lower than the values noted for the other two conditions. However, for R this is also the case, since for this environment this parameter is higher, even though it is not so evident. This could be caused by the scale of the graph of the R parameter in Fig. 12. The large increases in the non-linearity at 250 days of the R parameter (it is a ratio) for environments C and especially B, overshadow the possible differences at 28 days. Therefore, the newly proposed DIFA parameter and the comparison of the two parameters are very useful.

Finally, comparing the results of NLU and UPV measurements, the changes with time and the differences between the different environments observed for UPV were low, whereas more noticeable differences were reported for NLU parameters DIFA and R. This would suggest that they would be more sensitive than conventional UPV. Then, the non-linear ultrasonic measurements could be useful for getting consistent data about the evolution of microstructure of cementitious materials, at least matured under the analyzed conditions, improving the information provided by classical linear ultrasonic pulse velocity.

5. Conclusions

The main conclusions of this work can be summarised as follows.

- In general, lower total porosity, higher pore refinement and higher mechanical strengths were noted in the long term for mortars matured in the optimum laboratory condition, compared to those kept in non-optimum environments. This may be a consequence of the high humidity present in the optimum condition which facilitated the clinker hydration. At later ages, for the real outdoor and non-optimum laboratory environments, the lower relative humidity available would hinder the clinker hydration and it could also produce the appearance of shrinkage microcracking. This may lead to a loss of microstructure refinement and to a worsening of mechanical performance of the mortars.
- The differences regarding ultrasonic pulse velocity of mortars between the analyzed environments were lower than those observed for other studied parameters. Despite that, the evolution of this parameter with time for each environment was generally compatible with that observed for other studied parameters.
- The results of parameters R and DIFA obtained with non-linear ultrasonic measurements for the studied environments were overall in keeping with those related to microstructure characterization and mechanical strengths. In particular, it has been observed an adequate correlation between parameter DIFA and the pore size distributions determined using mercury porosimetry.
- In view of the results obtained, the non-linear ultrasonic measurements could be useful for obtaining reliable information with regard to the evolution of microstructure of cement-based materials, at least exposed to the studied environments, improving the information provided by classical linear ultrasonic pulse velocity.

Declaration of competing interest

The authors declare that they have no known competing financial interests or personal relationships that could have appeared to influence the work reported in this paper.

Acknowledgements

This research has been financially supported by the Conselleria de Educación, Investigación, Cultura y Deporte (currently re-named as Conselleria de Innovación, Universidades, Ciencia y Sociedad Digital) of Generalitat Valenciana (Spain) through the project code GV/2019/070 and by the Ministerio de Ciencia e Innovación of Spain through the project code RTC2019-006964-3. Part of the results presented in this manuscript was obtained in the PhD thesis carried out by Javier Ibáñez-Gosálvez at University of Alicante (Spain). Authors express their gratitude to Cementos Portland Valderrivas S.A. for supplying the Portland cement CEM I 42.5 R used in this work.

References

AENOR, UNE-EN 197-1:2011, 2000. Composición, especificaciones y criterios de conformidad de los cementos comunes, p. 30.
AENOR, UNE-EN 1015-11:1999, 1999. Métodos de ensayo de los morteros para albañilería. Parte 11. Determinación de la resistencia a flexión y a compresión del mortero endurecido, p. 16.
Aenor UNE–EN 12504–4, 2006. Ensayos de hormigón en estructuras. Parte 4. Determinación de la velocidad de los impulsos ultrasónicos, p. 18.
AENOR, UNE-EN 196-1:2005, 2005. Métodos de ensayo de cementos. Parte 1. Determinación de resistencias mecánicas.
Ahn, E., Kim, H., Sim, S.-H., Shin, S.W., Popovics, J.S., Shin, M., 2018. Surface-wave based model for estimation of discontinuity depth in concrete. Sensors 18. https://doi.org/10.3390/s18092793.
Ahn, E., Kim, H., Gwon, S., Oh, S.-R., Kim, C.-G., Sim, S.-H., Shin, M., 2022a. Monitoring of self-healing in concrete with micro-capsules using a combination of air-coupled surface wave and computer-vision techniques. Struct. Health Monit. 21, 1661–1677. https://doi.org/10.1177/14759217211041002.
Ahn, E., Shin, M., Popovics, J.S., 2022b. Air-coupled ultrasonic diffuse-wave techniques to evaluate distributed cracking damage in concrete. Ultrasonics 125. https://doi.org/10.1016/j.ultras.2022.106800.
Atiş, C.D., 2003. Accelerated carbonation and testing of concrete made with fly ash. Construct. Build. Mater. 17, 147–152. https://doi.org/10.1016/S0950-0618(02)00116-2.
Aymerich, F., Staszewski, W.J., 2010. Experimental study of impact-damage detection in composite laminates using a cross-modulation vibro-acoustic technique. Struct. Health Monit. 9, 541–553. https://doi.org/10.1177/1475921710365433.
Berriman, J., Purnell, P., Hutchins, D.A., Neild, A., 2005. Humidity and aggregate content correction factors for air-coupled ultrasonic evaluation of concrete. Ultrasonics 43, 211–217. https://doi.org/10.1016/j.ultras.2004.07.003.
Bingöl, A.F., Tohumcu, İ., 2013. Effects of different curing regimes on the compressive strength properties of self compacting concrete incorporating fly ash and silica fume. Mater. Des. 51, 12–18. https://doi.org/10.1016/j.matdes.2013.03.106.

Biondi, S., Valente, C., Zuccarino, L., 2017. Water content effect on concrete response in UPV tests. In: Santhanam, M., Gettu, R., Pillai, R.G., Nayar, S.K. (Eds.), Proc. 71st RILEM Annu. Week ICACMS 2017. RILEM Publications S.A.R.L., Chennai,India, pp. 338–343.
Çakır, Ö., Aköz, F., 2008. Effect of curing conditions on the mortars with and without GGBFS. Construct. Build. Mater. 22, 308–314. https://doi.org/10.1016/j.conbuildmat.2006.08.013.
Chalee, W., Jaturapitakkul, C., Chindaprasirt, P., 2009. Predicting the chloride penetration of fly ash concrete in seawater. Mar. Struct. 22, 341–353. https://doi.org/10.1016/j.marstruc.2008.12.001.
Chen, J., Wu, Y., Yang, C., 2019. Damage assessment of concrete using a non-contact nonlinear wave modulation technique. NDT E Int. 106, 1–9. https://doi.org/10.1016/j.ndteint.2019.05.004.
Climent, M.Á., Miró, M., Carbajo, J., Poveda, P., de Vera, G., Ramis, J., 2019. Use of non-linear ultrasonic techniques to detect cracks due to steel corrosion in reinforced concrete structures. Materials 12. https://doi.org/10.3390/MA12050813.
Climent, M.-Á., Miró, M., Eiras, J.-N., Poveda, P., de Vera, G., Segovia, E.-G., Ramis, J., 2022. Early detection of corrosion-induced concrete micro-cracking by using nonlinear ultrasonic techniques: possible influence of mass transport processes. Corros. Mater. Degrad. 3 https://doi.org/10.3390/cmd3020014.
Climent-Llorca, M.Á., Miró-Oca, M., Poveda-Martínez, P., Ramis-Soriano, J., 2020. Use of higher-harmonic and intermodulation generation of ultrasonic waves to detecting cracks due to steel corrosion in reinforced cement mortar. Int. J. Concr. Struct. Mater. 14 https://doi.org/10.1186/s40069-020-00432-x.
Dakel. IDK09, (n.d.). http://www.dakel.cz. (Accessed 3 July 2022).
de Grazia, M.T., Deda, H., Sanchez, L.F.M., 2021. The influence of the binder type & aggregate nature on the electrical resistivity of conventional concrete. J. Build. Eng. 43 https://doi.org/10.1016/j.jobe.2021.102540.
Del Río, L.M., Jiménez, A., López, F., Rosa, F.J., Rufo, M.M., Paniagua, J.M., 2004. Characterization and hardening of concrete with ultrasonic testing. Ultrasonics 42, 527–530. https://doi.org/10.1016/j.ultras.2004.01.053.
Den Abeele, K.E.A.V., Johnson, P.A., Sutin, A., 2000a. Nonlinear elastic wave spectroscopy (NEWS) techniques to discern material damage, Part I: nonlinear wave modula-tion spectroscopy (NWMS). Res. Nondestr. Eval. 12, 17–30. https://doi.org/10.1080/09349840009409646.
Den Abeele, K.E.A.V., Carmeliet, J., Ten Cate, J.A., Johnson, P.A., 2000b. Nonlinear elastic wave spectroscopy (NEWS) techniques to discern material damage, Part II: single-mode nonlinear resonance acoustic spectroscopy. Res. Nondestr. Eval. 12, 31–42. https://doi.org/10.1080/09349840009409647.
Detwiler, R.J., Kjellsen, K.O., Gjorv, O.E., 1991. Resistance to chloride intrusion of concrete cured at different temperatures 88, 19–24.
Diamond, S., 2000. Mercury porosimetry. Cement Concr. Res. 30, 1517–1525. https://doi.org/10.1016/S0008-8846(00)00370-7.
Donskoy, D., Sutin, A., Ekimov, A., 2001. Nonlinear acoustic interaction on contact interfaces and its use for nondestructive testing. NDT E Int. 34, 231–238. https://doi.org/10.1016/S0963-8695(00)00063-3.
Eiras, J.N., 2016. Studies on Non Linear Mechanical Wave Behavior to Characterize Cement Based Materials and its Durability. Universidad Politécnica de Valencia.
Eiras, J.N., Kundu, T., Popovics, J.S., Payá, J., 2018. Cement-based Material Characterization Using Nonlinear Single-Impact Resonant Acoustic Spectroscopy. NSIRAS). https://doi.org/10.1007/978-3-319-94476-0_12.
El-Dieb, A.S., 2007. Self-curing concrete: water retention, hydration and moisture transport. Construct. Build. Mater. 21, 1282–1287. https://doi.org/10.1016/j.conbuildmat.2006.02.007.
Escalante-Garcia, J.I., 2003. Nonevaporable water from neat OPC and replacement materials in composite cements hydrated at different temperatures. Cement Concr. Res. 33, 1883–1888. https://doi.org/10.1016/S0008-8846(03)00208-4.
European Committee for Standardization, 2004. EN 1992-1-1 Eurocode 2: Design of Concrete Structures - Part 1-1. General rules and rules for buildings, Brussels.
Fülöp, L., Ferreira, M., Tuhti, A., Rapaport, G., 2022. Assessing the challenges of condition assessment of steel-concrete (SC) composite elements using NDE. Case Stud. Constr. Mater. 16 https://doi.org/10.1016/j.cscm.2022.e00887.
für N E V, D.I., 1981. Deutsche Norm DIN 50008 Part 1.
Ghosh, P., Tran, Q., 2015. Correlation between bulk and surface resistivity of concrete. Int. J. Concr. Struct. Mater. 9, 119–132. https://doi.org/10.1007/s40069-014-0094-z.
Guyer, R.A., Johnson, P.A., 2009. Nonlinear Mesoscopic Elasticity: the Complex Behaviour of Rocks, Soil, Concrete. John Wiley & Sons, Inc., Hoboken, New Jersey, U.S.
Ho, L.S., Nakarai, K., Duc, M., Kouby, A.L., Maachi, A., Sasaki, T., 2018. Analysis of strength development in cement-treated soils under different curing conditions through microstructural and chemical investigations. Construct. Build. Mater. 166, 634–646. https://doi.org/10.1016/j.conbuildmat.2018.01.112.
Horpibulsuk, S., Rachan, R., Chinkulkijniwat, A., Raksachon, Y., Suddeepong, A., 2010. Analysis of strength development in cement-stabilized silty clay from microstructural considerations. Construct. Build. Mater. 24, 2011–2021. https://doi.org/10.1016/j.conbuildmat.2010.03.011.
In, C.-W., Schempp, F., Kim, J.-Y., Jacobs, L.J., 2015. A fully non-contact, air-coupled ultrasonic measurement of surface breaking cracks in concrete. J. Nondestr. Eval. 34 https://doi.org/10.1007/s10921-014-0272-6.
In, C.-W., Arne, K., Kim, J.-Y., Kurtis, K.E., Jacobs, L.J., 2017. Estimation of crack depth in concrete using diffuse ultrasound: validation in cracked concrete beams. J. Nondestr. Eval. 36 https://doi.org/10.1007/s10921-016-0382-4.
Kanna, V., Olson, R.A., Jennings, H.M., 1998. Effect of Shrinkage and Moisture Content on the Physical Characteristics of Blended Cement Mortars, 28, pp. 1467–1477.
Khan, M.I., Lynsdale, C.J., 2002. Strength, permeability, and carbonation of high-performance concrete. Cement Concr. Res. 32, 123–131. https://doi.org/10.1016/S0008-8846(01)00641-X.
Kim, G., In, C.-W., Kim, J.-Y., Kurtis, K.E., Jacobs, L.J., 2014. Air-coupled detection of nonlinear Rayleigh surface waves in concrete - application to microcracking detection. NDT E Int. 67, 64–70. https://doi.org/10.1016/j.ndteint.2014.07.004.
Kjellsen, K.O., Detwiler, R.J., Gjørv, O.E., 1991. Development of microstructures in plain cement pastes hydrated at different temperatures. Cement Concr. Res. 21, 179–189. https://doi.org/10.1016/0008-8846(91)90044-I.
Kogbara, R.B., Iyengar, S.R., Grasley, Z.C., Masad, E.A., Zollinger, D.G., 2015. Non-destructive evaluation of concrete mixtures for direct LNG containment. Mater. Des. 82, 260–272. https://doi.org/10.1016/j.matdes.2015.05.084.
Kundu, T., Eiras, J.N., Li, W., Liu, P., Sohn, H., Payá, J., 2019. In: Kundu, T. (Ed.), Fundamentals of Nonlinear Acoustical Techniques and Sideband Peak Count BT - Nonlinear Ultrasonic and Vibro-Acoustical Techniques for Nondestructive Evaluation. Springer International Publishing, Cham, pp. 1–88. https://doi.org/10.1007/978-3-319-94476-0_1.
Lafhaj, Z., Goueygou, M., Djerbi, A., Kaczmarek, M., 2006. Correlation between porosity, permeability and ultrasonic parameters of mortar with variable water/cement ratio and water content. Cement Concr. Res. 36, 625–633. https://doi.org/10.1016/j.cemconres.2005.11.009.
Lefever, G., Van Hemelrijck, D., Snoeck, D., Aggelis, D.G., 2022. Self-healing assessment of cementitious mortars through ultrasonic monitoring. Cem. Concr. Compos. 133 https://doi.org/10.1016/j.cemconcomp.2022.104683.
Lefever, G., Charkieh, A.S., Abbass, M., Van Hemelrijck, D., Snoeck, D., Aggelis, D.G., 2023. Ultrasonic evaluation of self-healing cementitious materials with superabsorbent polymers: mortar vs. concrete. Dev. Built Environ. 13 https://doi.org/10.1016/j.dibe.2022.100112.
Lencis, U., Korjakins, A., 2013. Moisture effect on the ultrasonic pulse velocity in concrete cured under normal conditions and at elevated temperature. Rigas Teh. Univ. Zinat. Raksti. 14, 71.
Ma, B. -g., Wen, X. -d., Wang, M. -y., Yan, J. -j., Xiao-jian, G., 2007. Drying shrinkage of cement-based materials under conditions of constant temperature and varying humidity. J. China Univ. Min. Technol. 17, 428–431. https://doi.org/10.1016/S1006-1266(07)60119-9.
Miró, M., Eiras, J.N., Poveda, P., Climent, M.Á., Ramis, J., 2021. Detecting cracks due to steel corrosion in reinforced cement mortar using intermodulation generation of ultrasonic waves. Construct. Build. Mater. 286 https://doi.org/10.1016/j.conbuildmat.2021.122915.
Muller, M., Sutin, A., Guyer, R., Talmant, M., Laugier, P., Johnson, P.A., 2005. Nonlinear resonant ultrasound spectroscopy (NRUS) applied to damage assessment in bone. J. Acoust. Soc. Am. 118, 3946–3952. https://doi.org/10.1121/1.2126917.
Ohdaira, E., Masuzawa, N., 2000. Water content and its effect on ultrasound propagation in concrete - the possibility of NDE. Ultrasonics 38, 546–552. https://doi.org/10.1016/S0041-624X(99)00158-4.
Ortega, J.M., Sánchez, I., Cabeza, M., Climent, M.A., 2017. Short-term behavior of slag concretes exposed to a real in situ mediterranean climate environment. Materials 10. https://doi.org/10.3390/ma10080915.
Ospitia, N., Korda, E., Kalteremidou, K.-A., Lefever, G., Tsangouri, E., Aggelis, D.G., 2023. Recent developments in acoustic emission for better performance of structural materials. Dev. Built Environ. 13 https://doi.org/10.1016/j.dibe.2022.100106.
Ouellet, S., Bussière, B., Aubertin, M., Benzaazoua, M., 2007. Microstructural evolution of cemented paste backfill. Mercury intrusion porosimetry test results 37, 1654–1665. https://doi.org/10.1016/j.cemconres.2007.08.016.
Panzera, T.H., Rubio, J.C., Bowen, C.R., Vasconcelos, W.L., Strecker, K., 2008. Correlation between structure and pulse velocity of cementitious composites. Adv. Cement Res. 20, 101–108. https://doi.org/10.1680/adcr.2008.20.3.101.
Payan, C., Garnier, V., Moysan, J., Johnson, P.A., 2007. Applying nonlinear resonant ultrasound spectroscopy to improving thermal damage assessment in concrete. J. Acoust. Soc. Am. 121 https://doi.org/10.1121/1.2710745.
Payan, C., Garnier, V., Moysan, J., 2010. Effect of water saturation and porosity on the nonlinear elastic response of concrete. Cement Concr. Res. 40, 473–476. https://doi.org/10.1016/j.cemconres.2009.10.021.
Payan, C., Quiviger, A., Garnier, V., Chaix, J.F., Salin, J., 2013. Applying diffuse ultrasound under dynamic loading to improve closed crack characterization in concrete. J. Acoust. Soc. Am. 134 https://doi.org/10.1121/1.4813847.
Pedeferri, P., Bertolini, L., 2000. La durabilità del calcestruzzo armato. Mc Graw-Hill Education, Milano, Italy.
Pieczonka, L., Klepka, A., Martowicz, A., Staszewski, W.J., 2016. Nonlinear vibroacoustic wave modulations for structural damage detection: an overview. Opt. Eng. 55 https://doi.org/10.1117/1.OE.55.1.011005.
Quiviger, A., Payan, C., Chaix, J.-F., Garnier, V., Salin, J., 2012. Effect of the presence and size of a real macro-crack on diffuse ultrasound in concrete. NDT E Int. 45, 128–132. https://doi.org/10.1016/j.ndteint.2011.09.010.
Ramezanianpour, A.A., Malhotra, V.M., 1995. Effect of curing on the compressive strength, resistance to chloride-ion penetration and porosity of concretes incorporating slag. fly ash or silica fume 17, 125–133. https://doi.org/10.1016/0958-9465(95)00005-W.
Revilla-Cuesta, V., Shi, J.-Y., Skaf, M., Ortega-López, V., Manso, J.M., 2022. Non-destructive density-corrected estimation of the elastic modulus of slag-cement self-compacting concrete containing recycled aggregate. Dev. Built Environ. 12 https://doi.org/10.1016/j.dibe.2022.100097.
Scalerandi, M., Griffa, M., Antonaci, P., Wyrzykowski, M., Lura, P., 2013. Nonlinear elastic response of thermally damaged consolidated granular media. J. Appl. Phys. 113 https://doi.org/10.1063/1.4801801.

Shah, A.A., Ribakov, Y., 2009. Non-linear ultrasonic evaluation of damaged concrete based on higher order harmonic generation. Mater. Des. 30, 4095–4102. https://doi.org/10.1016/j.matdes.2009.05.009.

Shattaf, N.R., Alshamsi, A.M., Swamy, R.N., 2001. Curing/environment effect on pore structure of blended cement concrete. J. Mater. Civ. Eng. 13, 380–388. https://doi.org/10.1061/(ASCE)0899-1561(2001)13:5(380).

Shui, Z., Xuan, D., Wan, H., Cao, B., 2008. Rehydration reactivity of recycled mortar from concrete waste experienced to thermal treatment. Construct. Build. Mater. 22, 1723–1729. https://doi.org/10.1016/j.conbuildmat.2007.05.012.

Stauffer, J.D., Woodward, C.B., White, K.R., 2005. Nonlinear ultrasonic testing with resonant and pulse velocity parameters for early damage in concrete. ACI Mater. J. 102, 118–121.

Tanyidizi, H., Coskun, A., 2008. Determination of the principal parameter of ultrasonic pulse velocity and compressive strength of lightweight concrete by using variance method. Russ. J. Nondestr. Test. 44, 639–646. https://doi.org/10.1134/S1061830908090088.

Taylor, H.F.W., 1997. Cement Chemistry, second ed. Thomas Telford Publishing, London, UK.

Thomas, M.D., Matthews, J., 2004. Performance of pfa concrete in a marine environment—10-year results. Cem. Concr. Compos. 26, 5–20. https://doi.org/10.1016/S0958-9465(02)00117-8.

Thomas, M.D.A., Scott, A., Bremner, T., Bilodeau, A., Day, D., 2008. Performance of slag concrete in marine environment. ACI Mater. J. 105, 628–634. http://www.scopus.com/inward/record.url?eid=2-s2.0-57149145850&partnerID=tZOtx3y1.

Trtnik, G., Turk, G., Kavčič, F., Bosiljkov, V.B., 2008. Possibilities of using the ultrasonic wave transmission method to estimate initial setting time of cement paste. Cement Concr. Res. 38, 1336–1342. https://doi.org/10.1016/j.cemconres.2008.08.003.

V Venkata, R., Mahindrakar, A.B., 2017. Impact of aggressive environment on concrete - a review. Int. J. Civ. Eng. Technol. 8, 777–788. https://www.scopus.com/inward/record.uri?eid=2-s2.0-85029908725&partnerID=40&md5=918ff9172ebecdecc28af9684c6cee4b.

Van Den Abeele, K., De Visscher, J., 2000. Damage assessment in reinforced concrete using spectral and temporal nonlinear vibration techniques. Cement Concr. Res. 30, 1453–1464. https://doi.org/10.1016/S0008-8846(00)00329-X.

Warnemuende, K., Wu, H.-C., 2004. Actively modulated acoustic nondestructive evaluation of concrete. Cement Concr. Res. 34, 563–570. https://doi.org/10.1016/j.cemconres.2003.09.008.

Williams, M., Ortega, J.M., Sánchez, I., Cabeza, M., Climent, M.Á., 2017. Non-destructive study of the microstructural effects of sodium and magnesium sulphate attack on mortars containing silica fume using impedance spectroscopy. Appl. Sci. 7 https://doi.org/10.3390/app7070648.

Wu, H.C., Warnemuende, K., 2005. How cracks modulate nonlinear acoustic signals. In: In: 11th Int. Conf. Fract. 2005, ICF11, pp. 1560–1565.

Xue, S., Zhang, P., Wang, J., Bao, J., Han, S., He, L., 2021. Influences of thermal damage on water transport in heat-treated cement mortar: experimental and theoretical analyses. Construct. Build. Mater. 288 https://doi.org/10.1016/j.conbuildmat.2021.123100.

Yildirim, H., Sengul, O., 2011. Modulus of elasticity of substandard and normal concretes. Construct. Build. Mater. 25, 1645–1652. https://doi.org/10.1016/j.conbuildmat.2010.10.009.

Zhang, J., Qin, L., Li, Z., 2009. Hydration monitoring of cement-based materials with resistivity and ultrasonic methods. Mater. Struct. Constr. 42, 15–24. https://doi.org/10.1617/s11527-008-9363-0.

Zhang, Y., Larose, E., Moreau, L., d'Ozouville, G., 2018. Three-dimensional in-situ imaging of cracks in concrete using diffuse ultrasound. Struct. Health Monit. 17, 279–284. https://doi.org/10.1177/1475921717690938.